Ionizational instability in an ionized inert gas flowing in a magnetic field

R. V. Vasil'eva, A. V. Erofeev,* E. A. D'yakonova, T. A. Lapushkina, and S. A. Poniaev
Ioffe Physico-Technical Institute, Russian Academy of Sciences, St. Petersburg, 194021, Russia
(Received 6 October 2000; published 26 February 2001)

We discuss the evolution of ionization instability, which gives rise to the formation of regular structures in plasma. The experiment was conducted in a disk magnetohydrodynamic channel in Xe. The evolution of luminous inhomogeneities, and changes in the luminosities of individual inhomogeneities, are traced. Electron concentrations and temperatures in fluctuations are measured. Average values of the electron concentration and temperature, plasma conductivity, and the Hall parameter are estimated. The average conductivity and Hall parameter are compared with the effective values. The influence of positive and negative fluctuations in plasma parameters on the enhancement of ionization oscillations and average current is analyzed. Based on experimental data, a mechanism is suggested that is responsible for the increase in the effective conductivity of ionizationally unstable inert gas plasma with increasing magnetic induction.

DOI: 10.1103/PhysRevE.63.036402 PACS number(s): 52.35.−g, 52.25.Gj, 52.30.−q

I. INTRODUCTION

It is known [1–4] that ionization (electrothermal) instability develops in closed-cycle magnetohydrodynamic (MHD) generator ducts earlier than other types of instability, and, therefore, can exert a greater influence on the channel characteristics. Experiments with generators of this type typically employ inert gases with an alkali metal seed as a working substance [3–6]. Since the development of ionization instability in these mixtures leads to decreasing effective plasma conductivity [7] and, hence, adversely affects energy conversion, a method for the suppression of ionization instability has been suggested [8]. Another approach to a solution of this problem involves the search for other conditions or working substances, the ionization instability of which can be favorable for energy conversion. One of these substances is an inert gas without an alkali seed, which can prove suitable for nonequilibrium MHD generators [9–12]. From a physical point of view, the major difference between an inert gas and an alkali metal lies in the structure of the atomic energy levels, and, as a result, these substances have different kinetic laws of ionization and recombination [13]. For instance, under MHD channel conditions, the characteristic time of three-particle recombination in inert gases can be several orders of magnitude longer than that in alkali metals. Our experiments [9,14–18] demonstrated that the evolution of ionization instability in a plasma of pure inert gases resulted in an increasing effective conductivity, which seemed surprising. The goal of the study described in this paper was to gain a deeper insight into this phenomenon. To this end, it was necessary to find the interrelationship between the structure of the inhomogeneities, the distribution of the plasma parameters, and integral characteristics of the MHD channel. Based on the obtained results, a physical model explaining how ionization and recombination kinetics affect the ionization instability evolution and plasma conductivity could be built, and the mechanisms responsible for the increase in the effective conductivity of the ionizationally unstable inert gas plasma could be revealed.

II. EXPERIMENTAL SETUP

The experimental setup consisted of a shock tube with a disc MHD channel 0.32 m in diameter and 0.01 m high. The maximum magnetic induction was 1.4 T. The experiment was conducted in Xe at a Mach number of the incident shock wave of 6.9, and under an initial pressure of 26 Torr. The channel is shown schematically in Fig. 1. For a more detailed description of the setup, see Refs. [9,14].

In a disk channel, the MHD interaction gives rise to an azimuthal Faraday current and a radial Hall field. Ohm's law for a Faraday channel with ideally segmented electrodes is given by

$$E_\varphi = kUB, \quad j_\varphi = -\sigma(1-k)uB, \quad j_r = 0,$$
$$E_r = \beta(E_\varphi - uB),$$

where u is the flow velocity, B is the magnetic field induction, σ is the plasma conductivity, β is the Hall parameter, and indexes φ and r refer to the azimuthal and radial directions, respectively, $E_{\varphi,r}$ is the electric field strength, $j_{\varphi,r}$ is the current density, and k is the load coefficient. Two configurations of the setup were used. In the first—

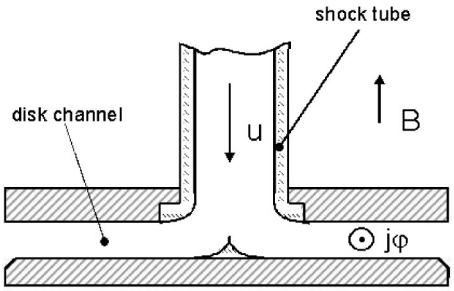

FIG. 1. Schematic representation of a disk MHD channel with a shock tube. B is the magnetic field, u the flow velocity, and j_φ the azimuthal current.

*Present address: Ioffe Physico-Technical Institute, St. Petersburg, 194021, Russia.
Email address: alex.erofeev@pop.ioffe.rssi.ru

electrodeless—configuration, a ring current was induced, i.e., the duct was operated as a short-circuited ($k=0$) Faraday channel with ideally segmented electrodes. In the second configuration, a narrow insert in the form of a sector with three pairs of electrodes, to which a load resistance was connected, was placed into the channel. In the experiment the load coefficient was in the range $0 \leqslant k \leqslant 0.2$. In our earlier papers [9,14–19] the interested reader can find a description of the procedures used for determining the gas-dynamic flow field; measuring the effective plasma conductivity, the Hall parameter, the electron concentration and temperature; and detecting luminous inhomogeneities.

III. BASIC PLASMA CHARACTERISTICS

The MHD interaction results in a separation of temperatures of electrons T_e and the heavy plasma component T_h. The temperature separation can be described by an expression similar to the Kerrebrok formula [2] which is obtained by transforming the balance equation for electron energy,

$$\frac{T_e - T_h}{T_h} = \frac{\gamma k_\sigma \beta^2 M^2 (1-k)^2}{3\delta}, \tag{1}$$

where $\gamma = c_p / c_v$, M is the Mach number of the flow, k_σ is a correction multiplier used in conductivity calculations [20], and δ is the inelastic loss factor which is mainly associated with the energy spent on gas ionization. The theory of the ionization kinetics of inert gases was developed in Ref. [13]. According to this, at temperatures typical of the MHD channel, the basic ionization mechanism can be described in a simplified manner as follows. The ionization rate is governed by the rate of excitation of lower energy levels by an electron impact. As stated by the principle of detailed balance, the recombination rate is determined by the reverse process. For instance, at $T_e = 8000$ K (which was characteristic of our experiment), the three-particle recombination coefficient in Xe is $K_r = 5 \times 10^{-41}$ m^6/s. If the electron concentration $n_e = 10^{21}$ m^{-3}, the characteristic recombination time under these conditions must be 2×10^{-2} s. Note that the flight time was of the order of 10^{-4} s.

In our experiment, the temperature separation was $T_e / T_h \leqslant 4$. In the absence of a magnetic field, the gas ionization degree α in the recombining plasma proved to be higher than the equilibrium value α_{eq} ($\alpha / \alpha_{eq} > 1$) because of slow recombination. When a magnetic field was applied, the processes of ionization began to dominate due to selective electron heating, i.e., the ratio between the nonequilibrium and equilibrium ionization degrees became less than unity, $\alpha / \alpha_{eq} < 1$.

For the gas ionization degrees realized in our MHD channel ($2 \times 10^{-4} < \alpha < 2 \times 10^{-3}$), the electron velocity distribution can be assumed to be Maxwellian [13]. Another characteristic of the plasma, which is important for a proper understanding of the experiment, is the ratio between the impulse transfer frequencies in collision with ions $\langle \nu_{ei} \rangle$ and atoms $\langle \nu_{ea} \rangle$:

$$\langle \nu_{ea} \rangle = n_a \langle c_e \rangle \langle Q_{ea} \rangle, \quad \langle \nu_{ei} \rangle = n_i \langle c_e \rangle \langle Q_{ei} \rangle,$$

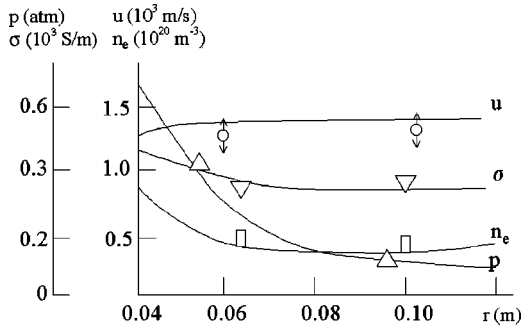

FIG. 2. Radial distribution of the flow velocity (u), conductivity (σ), electron concentration (n_e), and pressure (p). $B = 0.25$ T. The curves show calculated values, the points the experimental results. The circles indicate the flow velocity, down triangles mark the conductivity, squares show the electron concentration, and up triangles show the pressure.

$$\langle \nu \rangle = \langle \nu_{ea} \rangle + \langle \nu_{ei} \rangle.$$

Here n_a and n_i are the concentrations of atoms and ions, respectively; $\langle c_e \rangle$ is the average integral velocity of the electrons; and $\langle Q_{ea} \rangle$ and $\langle Q_{ei} \rangle$ are the impulse transfer cross sections in collision with atoms and ions averaged over the Maxwellian distribution, respectively. The ratio between $\langle \nu_{ei} \rangle$ and $\langle \nu_{ea} \rangle$ depends on the role of Coulomb collisions, which becomes greater with increasing ionization degree. In our experiment, $0.2 < \langle \nu_{ei} \rangle / \langle \nu_{ea} \rangle < 1$. Thus, because of a significant contribution of Coulomb collisions to the average impulse transfer frequency $\langle \nu \rangle$, it becomes dependent not only on the electron temperature but also the concentration, and this can affect the dependence of the Hall parameter on magnetic induction.

In calculations of the conductivity tensor components, the complicated dependence of the impulse transfer cross section on the electron energy in collision with atoms, and the role of Coulomb collisions, were taken into account, according to Ref. [20], by introducing coefficients k_σ and k_β, which are functions of n_a, n_e, T_e and B;

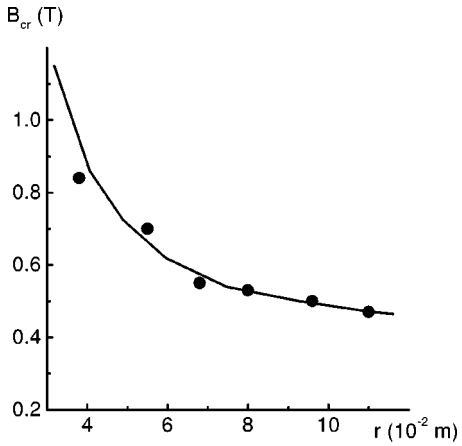

FIG. 3. Critical magnetic field as a function of the channel radius.

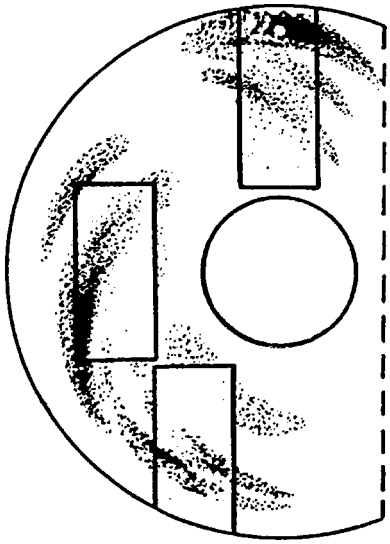

FIG. 4. Observation of luminous inhomogeneities. The rectangles show the strata fragments photographed through mirrors; the strata outside the rectangles were reconstructed by analyzing a sequence of frames.

$$\sigma = k_\sigma \frac{e^2 n_e}{m_e \langle \nu \rangle}, \quad \beta = k_\beta \frac{\omega_e}{\langle \nu \rangle}$$

where e is the electron charge, m_e is the electron mass, and $\omega_e = eB/m_e$.

The full set of equations describing the motion of a two-temperature stable plasma with nonequilibrium ionization in a disk MHD channel, and the method for a determination of initial conditions, were given in Ref. [9]. The one-dimensional radial expansion of the flow begins at $r = 0.04$ m, which was thought of as the disk channel inlet. The parameters at the channel inlet were flow velocity $u = 1.27 \times 10^3$ m/s, gas density $\rho = 0.45$ kg/m^3, heavy component temperature $T_a = 2600$ K, electron temperature $T_e = 3100$ K, ionization degree $\alpha = 2.6 \times 10^{-4}$, and Mach flow number $M = 2.45$. Figure 2 shows radial distributions of some plasma flow parameters for a weak MHD interaction $B = 0.25$ T. In the case of an unstable plasma it was assumed that plasma fluctuations did not result in considerable perturbations of the gas-dynamic parameters. To estimate changes in gas-dynamic parameters due to MHD deceleration of an unstable plasma, effective conductivities were used in the calculations.

An analysis of critical conditions of the ionization instability evolution, carried out in the linear approximation [21], showed that the critical Hall parameter appreciably depends on the plasma equilibrium degree α/α_{eq}. It was found that, at a low equilibrium degree $\alpha/\alpha_{eq} < 10^{-4}$, an instability can develop at any Hall parameter, however low. The lower the Hall parameter, the longer the time needed for the instability development. Calculations have shown that the angle between the wave vector and the electric current direction is in the range 90°–180°. The critical magnetic field B_{cr} was measured at various radii (Fig. 3). The critical magnetic induction B_{cr} was taken to be the induction at which fluctuations in the Hall parameter and plasma luminosity sharply increased. As is evident from Fig. 3, at the channel inlet, where the gas density is higher, the instability develops at higher magnetic induction than at the channel exit.

IV. LUMINOUS INHOMOGENEITIES

Dynamics of luminous inhomogeneities (magnetic strata) was studied by a high-speed filming of the disk channel segments. The magnetic strata pattern is shown in Fig. 4 for $B/B_{cr} = 2$. The fragments of the luminous layers, shown in Fig. 4 by rectangles, were observed using three mirrors placed at an angle of 45° to the disk surface. Using the sequence of frames, the entire pattern of the strata was reconstructed. Analysis of the data obtained with a high-speed motion-picture camera revealed that the strata were in the form of spokes making an angle of 20°–30° with the azimuthal direction, which means that the angle between the initial current and the wave vector was 110°–120°. The distance between the strata in the radial direction was about 0.03 m. Two or three strata were observed simultaneously in the disk. The strata appeared at intervals, and the strata propagation velocity was close to the flow velocity, i.e., it was as if the strata were frozen in the flow. When propagating in the channel, the strata became more luminous, somewhat wider, and better aligned with the initial current direction. Figure 5 presents photographic blackening in the radial direction. Here we can see the appearance of individual strata, and their increasing luminosity as they propagate in the channel. Attention is drawn to the fact that, once formed, the strata do not decay.

It is possible to follow the strata evolution in more detail by detecting temporal variations in electron concentration at different fixed locations in the channel. To this end, photo-

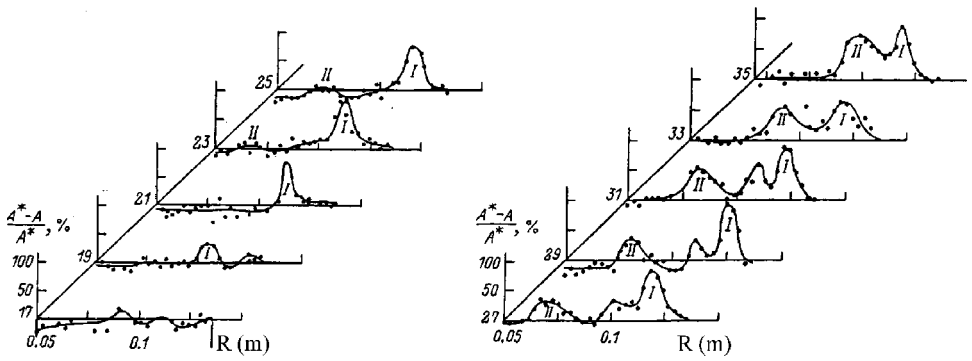

FIG. 5. Film blackening along the channel radius. A is the current reading of the microphotometer, and A^* is the current reading for the photographic fog. Roman numerals are the numbers of appearing strata, figures along the diagonal axis are the numbers of frames, and the time interval between frames is 3.2 μs.

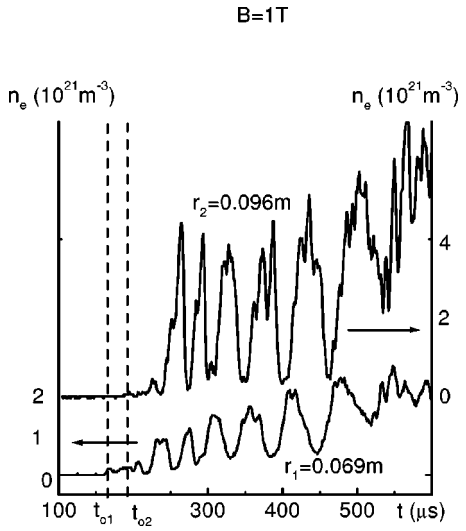

FIG. 6. Time variations in electron concentration at two locations along the channel radius for $B=1$ T. t_{01} and t_{02} are the times of the shock wave arrival into the first and second measuring sections, respectively.

multipliers were used to measure plasma luminosity through windows in the disk channel wall. Figure 6 demonstrates how the electron concentration changes at distances r_1 and r_2 as different volumes of plasma move past the measurement window. It can be seen that the time interval between the first electron concentration maxima is close to the time difference between the shock wave arrivals at r_1 and r_2, which suggests that the same strata are observed at r_1 and r_2. The electron concentration in the strata grows as they propagate downstream. The electron concentration distribution shown in Fig. 6 is seen to have large-scale inhomogeneities with a duration of 25–50 μs. During a flow time of 4.5×10^{-4} s, about eight large-scale strata pass through the channel. On their background, small-scale inhomogeneities, which are more pronounced at larger radii, are present. Here we find a certain analogy with the development of classical turbulence [22] when small-scale pulsations are regarded as a fine structure superimposed on a large-scale inhomogeneity.

V. ELECTRON CONCENTRATION AND TEMPERATURE

Figure 7 presents electron concentrations and temperatures in the inhomogeneities that move past the measurement window at $r=0.096$ m for $B=1$ T. It can be seen that, on the whole, large-scale regions with higher temperatures (strata) have higher electron concentrations and, conversely, that lower-temperature regions are characterized by lower electron concentrations, though the positions of the n_e and T_e maxima and minima are somewhat shifted. In the large-scale inhomogeneities, the highest and lowest electron concentrations differ by approximately a factor of 3–3.5, the electron temperature varying from 8500 to 7000 K. In the small-scale inhomogeneities, variations in the electron concentration are weaker by about 50%, while the temperature may rise as high as 10000–11000 K. The average value of T_e over fluctuations $\langle T_e \rangle$ is 7800 K. Measurements of electron temperatures T_e at radii r_1 and r_2 revealed that average temperatures at these radii were nearly equal.

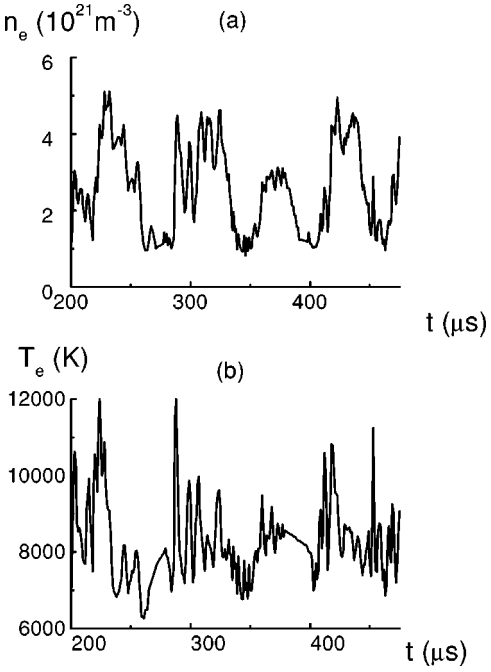

FIG. 7. Variations in inhomogeneities of electron concentration (n_e) and temperature (T_e) at a radius $r_2=0.096$ m.

Figure 8 shows electron temperatures averaged over fluctuations in the region (r_2-r_1). $\langle T_e \rangle$ was obtained by averaging the results of several experiments. Figure 8 also depicts the calculated $T_e=f(B)$ dependence for $B<B_{cr}$. It should be emphasized that an extension of the calculations made concerning the assumption of a stable plasma in the region of high magnetic fields yields a nonmonotonic $T_e=f(B)$ dependence. This can be explained by the fact that the role of Coulomb collisions grows as ionization develops. This gives rise to a higher energy transfer frequency and, hence, weaker selective electron heating. The measured average values of T_e in the ionizationally unstable plasma proved to be lower than those calculated on the assumption of stable plasma.

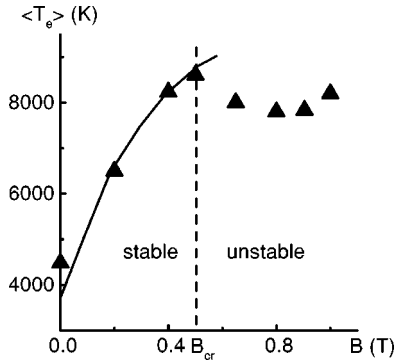

FIG. 8. Average electron temperature for various magnetic inductions. The points are the experimental values, and the curves show the temperatures calculated on the assumption of stable plasma.

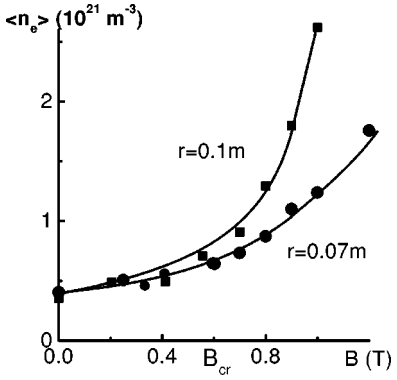

FIG. 9. Average electron concentration as a function of magnetic field for two radii.

Figure 9 demonstrates electron concentrations averaged over fluctuations for different magnetic fields at radii r_1 and r_2. Each point was obtained by processing several measurements. It can be seen that $\langle n_e \rangle$ grows in a radial direction with increasing B.

VI. IONIZATION RATE

Average ionization rates were estimated by processing measurements of $\langle n_e \rangle$ for two radii, $r_1 = 0.069$ m and $r_2 = 0.096$ m:

$$\frac{\Delta \langle n_e \rangle}{\Delta t} = \frac{\langle n_{e2} \rangle - \langle n_{e1} \rangle}{\Delta t} - \frac{\langle n_{e1} \rangle}{n_{a1}} \frac{n_{a2} - n_{a1}}{\Delta t}. \qquad (2)$$

The first (basic) term of the right-hand side of Eq. (2) was derived from the experimental data. The second term takes into account variations in the atomic concentration. As estimates have shown, this term is small compared with the first term, and therefore it could be obtained by calculations. Since the flow velocity u in this part of the channel changed only slightly, we obtained $\Delta t = (r_2 - r_1)/u$. Figure 10 shows ionization rates for different magnetic inductions. The average ionization rates derived in this fashion were compared with the ionization rates calculated for average measured electron temperatures,

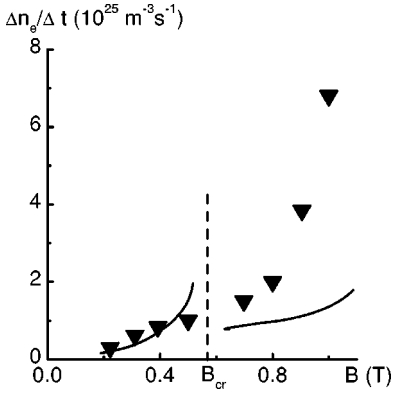

FIG. 10. Average ionization rate as a function of magnetic induction. The points are the experimental values, and the curves show the calculated ionization rates.

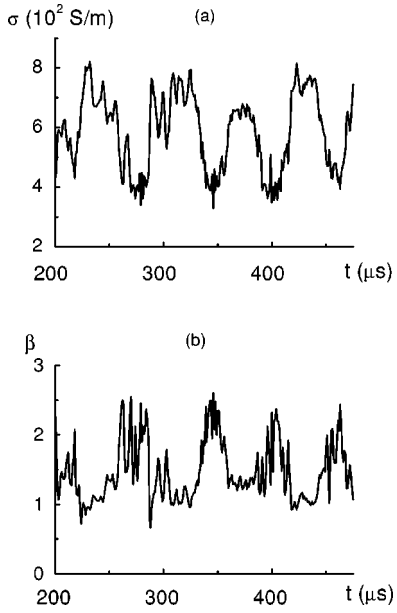

FIG. 11. Time variations in the local conductivity (σ) and Hall parameter (β).

$$\frac{d\langle n_e \rangle}{dt} = \langle n_e \rangle n_a \langle K_i \rangle - \langle n_e \rangle^3 \langle K_r \rangle - \frac{\langle n_e \rangle}{n_a} \frac{dn_a}{dt},$$

where $dt = dr/u$. The dependences of the ionization and recombination coefficients K_i and K_r on the electron temperature were taken from Ref. [13]. $\langle K_i \rangle$ and $\langle K_r \rangle$ were calculated for $T_e = \langle T_e \rangle$. Experimental values of $\langle n_{e1} \rangle$ were used as the initial values of $\langle n_e \rangle$ at $r = r_1$. The $n_a(t)$ dependence was obtained through calculations. It is evident from Fig. 10 that the measured ionization rates in the stable plasma region ($B < B_{cr}$) are lower than calculated. However, the discrepancy is within the limits of experimental error, because Δn_e in this region was determined as a small difference between large values. Conversely, in the ionizationally unstable plasma region ($B > B_{cr}$), the average ionization rates prove to be much greater than those calculated for average temperatures. It is likely that this is because a dominating contribution to the increase of the average electron concentration comes from regions with higher temperatures.

VII. CONDUCTIVITY AND HALL PARAMETER

Local values of the conductivity and Hall parameter were calculated from measured electron concentrations and temperatures and calculated atomic concentrations [20]. Figure 11 shows the $\sigma(t)$ and $\beta(t)$ dependences obtained by processing the $T_e(t)$ and $n_e(t)$ curves given in Fig. 7. Local values of σ change similarly to those of $T_e(t)$ and $n_e(t)$. This means that regions with higher T_e and n_e correspond to regions of higher conductivity and, conversely, that regions with lower T_e and n_e correspond to regions of lower conductivity. The Hall parameter is out of phase with the conductivity. This can be explained by the fact that under the conditions discussed here the role of Coulomb collisions is

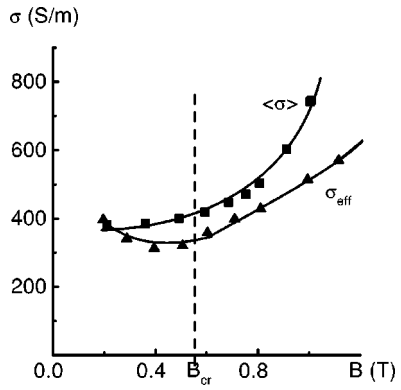

FIG. 12. Average and effective conductivities vs magnetic induction.

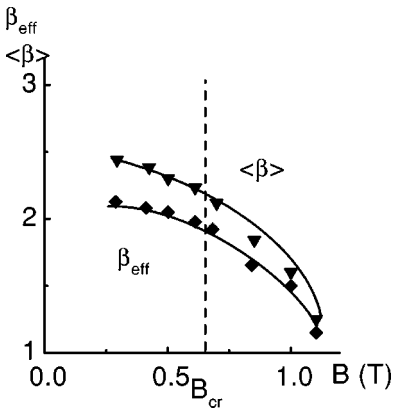

FIG. 13. Average and effective values of the Hall parameter vs magnetic induction.

rather large, and, as a consequence, the impulse transfer frequency grows with increasing n_e. Dependences of the type shown in Figs. 7 and 11 serve to determine average values of $\langle T_e\rangle$, $\langle n_e\rangle$, $\langle\sigma\rangle$, and $\langle\beta\rangle$. It is important to note that fluctuations in n_e, T_e, σ, and β, shown in Figs. 7 and 11, are fluctuations with respect to average values. The behavior of positive and negative fluctuations with respect to the initial undisturbed plasma conditions will be discussed below.

The onset of fluctuation currents due to the ionization instability evolution affects the average azimuthal current and average radial field. This implies that the integral characteristics of the MHD channel, such as the effective conductivity and effective Hall parameter, can differ from their average values. In our experiment, the effective conductivity σ_{eff} and the effective Hall parameter β_{eff} in a short-circuited Faraday channel (at $k=0$) were determined as $\sigma_{\text{eff}}=\langle j_\varphi\rangle/uB$ and $\beta_{\text{eff}}=\langle E_r\rangle/uB$.

Figure 12 shows average and effective conductivities for different magnetic fields. The relation between σ_{eff} and $\langle\sigma\rangle$ can be expressed as $\sigma_{\text{eff}}=\langle\sigma\rangle/(1+\xi)$, where ξ is the cofficient depending on the magnitude and direction of fluctuation currents [23]. It can be seen that $\langle\sigma\rangle$ and σ_{eff} are nearly equal at $B<B_{cr}$. At $B>B_{cr}$, they increase as the magnetic induction grows, but σ_{eff} grows more slowly than $\langle\sigma\rangle$. As stated above, σ_{eff} is affected by two factors: the structure of inhomegeneities and average conductivity. Our first observations of the increasing σ_{eff} in stratified plasma seemed surprising. However, as our data indicate, this can be explained by the fact that, in the competition between the plasma stratification and average conductivity increase, the latter dominates.

Figure 13 presents average and effective Hall parameters. According to Ref. [23], $\beta_{\text{eff}}=\langle\beta\rangle/(1+\eta)$, where η is the cofficient governed by the magnitude and direction of fluctuation electric fields. The drop in $\langle\beta\rangle$ with increasing magnetic induction is attributable to the fact that the electron concentration grows with increasing field, which leads to a greater average impulse transfer frequency and, hence, a falling β. Since the accuracy of the determination of $\langle\beta\rangle$ and β_{eff} was no better than 10%, we can assert that $\langle\beta\rangle$ and β_{eff} shown in Fig. 13 are nearly equal. As theory predicts [23], this situation can take place when inhomogeneities are almost parallel to the initial current direction.

VIII. ON THE ELECTRON ENERGY BALANCE

The electron energy balance is given by

$$\sigma_{\text{eff}}(uB)^2(1-k)^2=\frac{3m_e}{m_a}k\langle n_e\rangle\langle\nu\rangle(\langle T_e\rangle-T)+\left(E_i+\frac{5}{2}k\langle T_e\rangle\right)\frac{\langle\Delta n\rangle}{\Delta t}+\Delta W.$$

This expression shows that the Joule heating power W_J is spent on energy transfer to the heavy component in elastic and inelastic collisions (W_e and W_i, respectively), and also accounts for some additional losses referred to as the ''energy defect'' ΔW. The energy losses associated with the plasma radiation and excitation were ignored here because, as shown by estimates, they were small. Since major attention was paid to a comparison of the ''energy defect'' in the undercritical and overcritical magnetic fields, a simplified form of the equation for the electron energy balance could be used here.

Figure 14 demonstrates the Joule heating power W_J, the elastic energy losses W_e, and the energy needed for ionization W_i. Figure 15 presents the ratio between the ''energy defect'' ΔW and the Joule heating power W_J. The observed nonzero ratio $\Delta W/W_J$ at $B<B_{cr}$ is within the limits of ex-

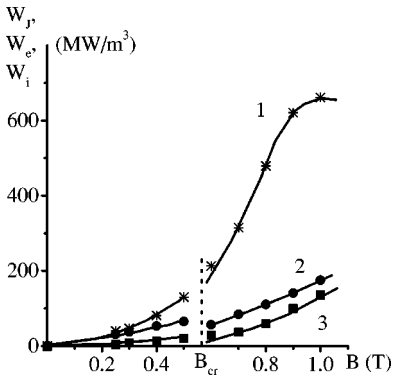

FIG. 14. Joule heating power W_J (1), elastic energy losses W_e (2), and energy spent on ionization W_i (3) for different magnetic inductions. B_{cr} is the critical magnetic field.

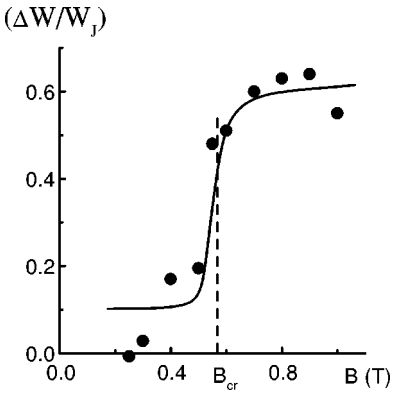

FIG. 15. Relative electron energy defect for various magnetic fields.

perimental accuracy. As soon as parameter fluctuations occur, the ''energy defect'' sharply increases. In an ionizationally unstable plasma the energy defect is about half the Joule heating power. This suggests that there are some types of electron energy loss in the fluctuations.

IX. SOME REMARKS ON DEVELOPMENT OF THE IONIZATION INSTABILITY

The nonlinear stage of the ionization instability evolution in inert gas at $\alpha < \alpha_{eq}$ was theoretically considered in Ref. [24] for the mixture Ar+Cs at $T_e \geqslant 5500$ K, when Ar ionization takes place. Based on the experimental evidence obtained in the work described here, we would like to present our understanding of ionization instability evolution in a relaxing plasma.

As a first approximation, let us present the structure of plasma inhomogeneities in a Cartesian coordinate system, where they are in the form of inclined bands. In disk geometry, the inhomogeneities would have this shape if they were observed at radii much larger than the initial radius. Note that the *Y* axis corresponds to the φ direction, and the *X* axis is the *r* direction. Figure 16 depicts the coordinate system and directions of the initial current j_0, the electric field strength E_0^* in the plasma, and the wave vector. The angle between j_0 and E_0^* is denoted by δ ($tg\,\delta = \beta$). The angle θ between j_0 and k (normal to the band) is in the range $\pi/2 < \theta < \pi$, since, as the experiment showed, the bands make an angle of 20°–30° with the initial current. The same vector

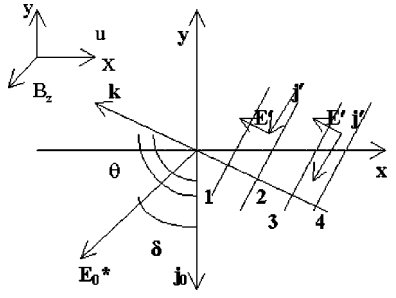

FIG. 16. Schematic representation of inhomogeneities and directions of main vectors.

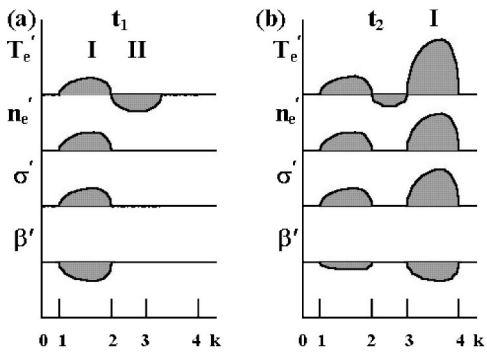

FIG. 17. Fluctuations in the electron temperature (T_e'), electron concentration (n_e'), conductivity (σ'), and Hall parameter (β') along the normal to inhomogeneities for two time moments.

directions were obtained in a solution of the theoretical problem of critical conditions for the ionization instabity in a relaxing plasma [21]. Let us denote the increments in the basic plasma parameters as $j' = j - j_0$, $\sigma' = \sigma - \sigma_0$, $\beta' = \beta - \beta_0$, $E' = E - E_0$, $T_e' = T_e - T_{e0}$, and $n_e' = n_e - n_{e0}$, where the index ''0'' indicates the values of the parameters in the undisturbed medium. For an unbounded plasma, the fluctuations in the current and electric field strength are related to the fluctuations in the conductivity and Hall parameter by [4,23]

$$j' = j_0(\sin\theta - \beta\cos\theta)\frac{\sigma'}{\sigma_0} + j_0\beta'\cos\theta; \tag{3}$$

$$\pm E' = -\frac{1+\beta_0^2}{\sigma_0} j_0 \cos\theta \frac{\sigma'}{\sigma_0} + \frac{j_0}{\sigma_0}(\sin\theta + \beta_0\cos\theta)\beta', \tag{4}$$

where ''+'' denotes coinciding directions of the E and k vectors, and ''−'' indicates opposite directions. Equation (3) shows that the fluctuation current enhancement in the j_0 direction is caused by positive fluctuations in σ and negative fluctuations in β. Figure 17 schematically shows disturbances in basic plasma parameters along the normal to the observed inhomogeneities. The numbers indicate the dimensionless distances along the normal corresponding to Fig. 16. Let us see how positive and negative fluctuations in the electron concentration and temperature behave. Let the fluctuation T_e, shown in Fig. 17(a), take place at a certain moment of time t_1. Since the characteristic ionization time [$(1-5)\times 10^{-5}$ s] in our experiment is much shorter than the lifetime of this inhomogeneity, the electron concentration will considerably rise in regions of high electron temperatures (I). In the low-temperature regions (II), the electron concentration will remain nearly equal to the initial one due to a slow three-particle recombination; the characteristic recombination time in the experimental conditions was on the order of 10^{-2} s, which is much greater than the flight time. Accordingly, the conductivity will grow in region I and remain nearly unaltered in region II. As seen in Fig. 17(a), increments in the Hall parameter can be opposite to the increments in σ. A positive increment in σ and negative incre-

ment in β lead to the fluctuation current enhancement in region I. The fluctuation current is added to the initial current, which leads to increasing effective conductivity. In turn, increasing the effective conductivity results in greater Joule heating and higher electron temperature and concentration. Thus it becomes evident that positive fluctuations in T_e and n_e lead to enhanced perturbations, while negative fluctuations do not show a tendency toward enhancement. To make the picture more clear, let us suppose that a negative fluctuation in n_e occurs. This will lead to a decrease in conductivity and, as predicted by Eq. (3), to a weaker Joule heating and a lower electron temperature T_e. However, no further decrease in the electron concentration n_e will occur due to slow recombination. During a time t_2-t_1 the plasma volume I occupying position 1-2 moves along the channel to position 3-4 [see Fig. 17(b)]. During this period positive fluctuations in T_e, n_e, and σ, and negative fluctuations in β, continue to develop during this time. At position 1-2, a new fluctuation arises during this time. In a bounded volume, the pattern of fluctuation currents differs considerably from that presented in Fig. 15. In part, fluctuation currents are short circuited inside the plasma, thus forming local eddy currents, which leads to an additional energy dissipation. In part, the fluctuation currents are closed in a manner similar to the basic current, thereby increasing the average current and the effective plasma conductivity.

X. CONCLUSIONS

Based on an analysis of our experimental data, the following explanation of specific features of the plasma flow in a MHD channel can be suggested. Selective heating of electrons and nonequlibrium ionization in the presence of the Hall effect give rise to the formation of regular inhomogeneities in the plasma, inclined at a definite angle to the initial current. The lifetime of inhomogeneities is larger than the flight time; it is as if they are frozen in the flow, and consist of regions with higher electron temperature and concentration and regions with lower electron temperature and concentration. Major changes in the plasma flow are experienced by the electron concentration: its average value and modulation depth increase with increasing magnetic field.

Since the characteristic ionization time is comparable to the flight time, and the characteristic recombination time is orders of magnitude larger than the flight time, the electron concentration reacts mainly to positive increments in the electron temperature, which leads to increasing conductivity. In turn, positive fluctuations in conductivity give rise to fluctuation currents in such a direction that they enhance the average current. All these factors create conditions for the preferential development of positive fluctuations in the electron concentration and temperature. Negative fluctuations in these parameters are suppressed because of the absence of a positive interrelationship between them due to relatively slow recombination. As a result, there occurs an increase in the effective conductivity with increasing magnetic field, as observed in the experiments.

The picture of ionization instability evolution obtained in our experiment can also take place in a large-scale MHD channel if the relationship between characteristic ionization and recombination times and the flight time is properly chosen. Therefore, if inert gases or their mixtures are used as a working substance in MHD generators, ionization instability can lead to increasing conversion efficiency.

ACKNOWLEDGMENT

The authors wish to thank Dr. V. A. Bityurin for helpful discussions.

[1] E.P. Velikhov and A.M. Dykhne, Proc. Compt. Rend. Conf. Int. Phenomenes Ionieat. Gas. Paris **4**, 511 (1963).
[2] J.L. Kerrebrock, AIAA J. **2** No. 6, 1072 (1964).
[3] R.J. Rosa, *Magnetohydrodynamic Energy Conversion* (McGraw-Hill, New York, 1968).
[4] A.V. Nedospasov and V. D. Khait, *Principles of the Physics of Processes in Low-Temperature Plasma Devices* (Energoatomizdat, Moscow, 1991).
[5] Y. Okuno *et al.*, in *Proceedings of International Conference on MHD Power Generation and High Temperature Technologies 1999, Beijing PRC* (IEE CAS, Beijing, 1999), Vol. 1, pp. 223–231.
[6] H. Yamasaki *et al.*, in *Proceedings of International Conference on MHD Power Generation and High Temperature Technologies 1999, Beijing PRC* (Ref. [5]), Vol. 1, pp. 233–241.
[7] A. Solbes, in *Proceedings Int. Conf. On MHD Power Generation, Warsaw, 1968* (IAAE, Warsaw, 1968), Vol. 1, p. 499.
[8] T. Nakamura and W. Reidmuller, AIAA J. **12**, 661 (1974).
[9] R.V. Vasil'eva *et al.*, *Low-Temperature Plasma of Inert Gases with Non-equilibrium Ionization and MHD Generators* (Ioffe PTI RAS, St. Petersburg, Russia, 1991), p. 206.
[10] R.V. Vasil'eva, A.V. Erofeev, and A.D. Zuev, in *Proceedings of the Eleventh International Conference on MHD Electrical Power Generation, Beijing, China, 1992* (IEE CAS, Beijing, 1992), Vol. IV, pp. 1199–1205.
[11] N. Harada, N. Sakamoto, and H. End, in *Proceedings of the 12th International Conference On Magnetohydrodynamic Electrical Power Generation. Yokohama, Japan, 1996* (TIT, Yokohama, 1996), Vol. 2, pp. 623–631.
[12] A.Y. Sokolov and Y. Okuno, in *Proceedings of the 34th Symposium on Engineering Aspects of Magnetohydrodynamics, Starkville, Mississippi, 1997* (UTSI, Mississippi, 1997), pp. 6.2.1.–6.2.14.
[13] L.M. Biberman, L.M. Vorob'ev, and V.S. Yakubov, *Kinetics of the Non-Equilibrium Low- Temperature Plasma* (Nauka, Moscow, 1982), p. 376.
[14] A.V. Erofeev, R.V. Vasil'eva, A.D. Zuev, T.A. Lapushkina, E.A. D'yakonova, and A.A. Markhotok, in *Proceedings of the 12th International Conference on Magnetohydrodynamic Electrical Power Generation, Yokohama, Japan, 1996* (Ref. [11]), Vol. 1, pp. 74–82.

[15] R.V. Vasil'eva, E.A. D'yakonova, A.V. Erofeev, A.D. Zuev, T.A. Lapushkina, and A.A. Markhotok, Zh. Tekh. Fiz. **67**, 6 (1997) [Tech. Phys. **42**, 1376 (1997)].

[16] T.A. Lapushkina, R.V. Vasil'eva, A.V. Erofeev, and A.D. Zuev, Zh. Tekh. Fiz. **67**, 12 (1997) [Tech. Phys. **42**, 1381 (1997)].

[17] R.V. Vasil'eva, E.A. D'yakonova, A.V. Erofeev, and T.A. Lapushkina, Zh. Tekh. Fiz. **69**, 56 (1999) [Tech. Phys. **44**, 1312 (1999)].

[18] E.A. D'yakonova, A.V. Erofeev, T.A. Lapushkina, and R.V. Vasil'eva, in *Proceedings of the International Conference on MHD Power Generation and High Temperature Technologies 1999, Beijing PRC, 1999* (IEE CAS, Beijing, 1999), Vol. I, pp. 299–307.

[19] T.A. Lapushkina, E.A. D'yakonova, and R.V. Vasil'eva, Pis'ma Zh. Tekh. Fiz. **24**, 58 (1998) [Tech. Phys. Lett. **24**, 66 (1998)].

[20] V.A. Brzhezitskii, Teplofiz. Vys. Temp. **10**, 7 (1972) [High Temp. **10**, 6 (1972)].

[21] R.V. Vasil'eva and A.V. Erofeev, Zh. Tekh. Fiz. **61**, 47 (1991) [Tech. Phys. **36**, 398 (1991)].

[22] L.D. Landau and E.M. Lifshits, *Mechanics of Continuous Medium* (State Publishing House of Technico-theoretical Literature, Moscow, 1954).

[23] L.A. Vulis, A.L. Genkin, and V.A. Fomenko, *Theory and Calculation of Magnetohydrodynamic Flows in Channels* (Atomizdat, Moscow, 1971).

[24] A.Y. Sokolov and S. Kabashima, in *Proceedings of the 12th International Conference on Magnetohydrodynamic Electrical Power Generator, Yokohama, Japan, 1996* (Ref. [11]), Vol. 2, pp. 751–761.